ACS NANO

www.acsnano.org

Article

Resonance Tuning of Localized Excitons via a Plasmonic Nanocavity

Qifa Wang, Guodong Xue, Cheng Ji, Yuxin Li, Chenyang Li, Liping Hou, Xiaobing Zheng, Qinghong Yu, Chaojie Ma,* Xuetao Gan, Kaihui Liu,* Jianlin Zhao, and Fajun Xiao*

Cite This: *ACS Nano* 2026, 20, 6279−6286

Read Online

ACCESS | Metrics & More | Article Recommendations | Supporting Information

ABSTRACT: In monolayer semiconductors, excitons confined by strain-induced potential traps are promising candidates for on-chip single-photon sources. For these quantum emitters, achieving broadband tunability while preserving high brightness is crucial for quantum information processing and communication, but remains challenging in aligning the emitter energy with optical resonances. Here, we demonstrate resonant tuning of localized exciton emission in monolayer WSe_2 using an Au nanocube-on-mirror nanocavity. The design enables simultaneous strain-induced exciton energy tuning and Purcell-enhanced emission. By adjusting the cavity gap, it allows precise spectral alignment of the localized exciton with the plasmonic resonance. We observe a record-large redshift over 240 meV in localized exciton energy. Compared with the conventional approach, a 22-fold enhancement in emission intensity is achieved due to the spectral, spatial, and polarization matching between the localized exciton and plasmons. Our findings establish a robust strategy for developing high-performance nonclassical light sources, facilitating the development of scalable quantum applications.

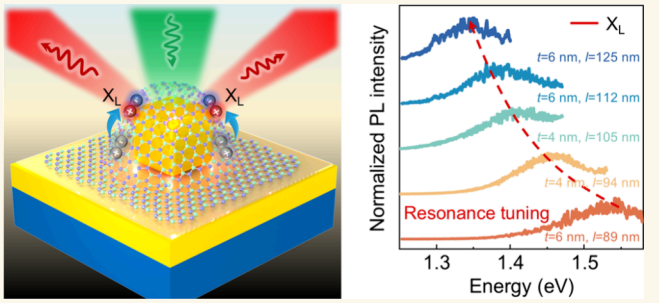

KEYWORDS: *plasmonic nanocavity, monolayer WSe_2, localized excitons, strain, Purcell effect*

Excitonic complexes in two-dimensional (2D) transition metal dichalcogenides (TMDs) play a pivotal role in driving intense light-matter interactions, offering tremendous potential for the development of future photonic and optoelectronic devices. Among the intensively studied free excitons, such as neutral excitons, trions, and biexcitons, remarkable progress has been made in their applications to light-emitting diodes (LEDs),[1] solar cells,[2] and valleytronic devices.[3] Apart from free excitons, localized excitons, arising from spatial confinement due to defects,[4] disorder,[5] or strain,[6−8] offer a promising path for advanced quantum technologies. Due to their long lifetimes,[9] robust spin-valley coupling,[10,11] and efficient photon extraction,[12,13] localized excitons are ideal candidates for the realization of single-photon emitters, which are essential building blocks for future on-chip quantum systems. Tuning the emission energy of localized excitons further enhances their potential, enabling possibilities for quantum information and communication. Recent advancements have demonstrated the manipulation of localized exciton energy via electrical and magnetic methods.[14−16] Nevertheless, these approaches heavily rely on cryogenic-temperature operations and complex device designs, limiting their scalability and practical integration into photonic on-chip devices.

Alternatively, the optical properties of localized excitons in 2D TMDs can be precisely manipulated by local tensile strain, which can be induced using on-chip compatible nanostressors such as particles,[17−21] pillars,[12,22−24] tips,[25,26] and holes.[15,27] Owing to their flexibility and strong intralayer bonding, 2D TMDs can endure strains of several percent without fracturing,[8,28] offering the potential for tuning localized excitons across a wide energy range. In particular, metallic stressors with large strain and strong plasmon resonance hold the promise to prevent thermally induced exciton delocalization while simultaneously enhancing quantum yields through the Purcell effect.[17,18,25] This results in stronger localized exciton emission, even at room temperature.

Researchers have demonstrated that the sharp tips of bowtie nanoantennas can create a highly confined potential in WSe_2 monolayers that localizes excitons at room temperature.[25] Further collaboration with tip-enhanced techniques has enabled significant Purcell-enhanced exciton emission, facilitating dynamic energy tuning with nanoscale spatial resolution. More recently, chemically synthesized metallic nanocrystals have been explored as stressors to ensure *in situ* coupling between plasmonic resonance and local strain in monolayer WS_2.[18] This approach offers a geometry-modulated mechanism for controlling localized exciton emission across a broader

Received: December 8, 2025
Revised: February 4, 2026
Accepted: February 6, 2026
Published: February 11, 2026

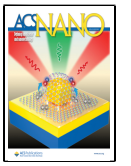

https://doi.org/10.1021/acsnano.5c21481
ACS Nano 2026, 20, 6279−6286

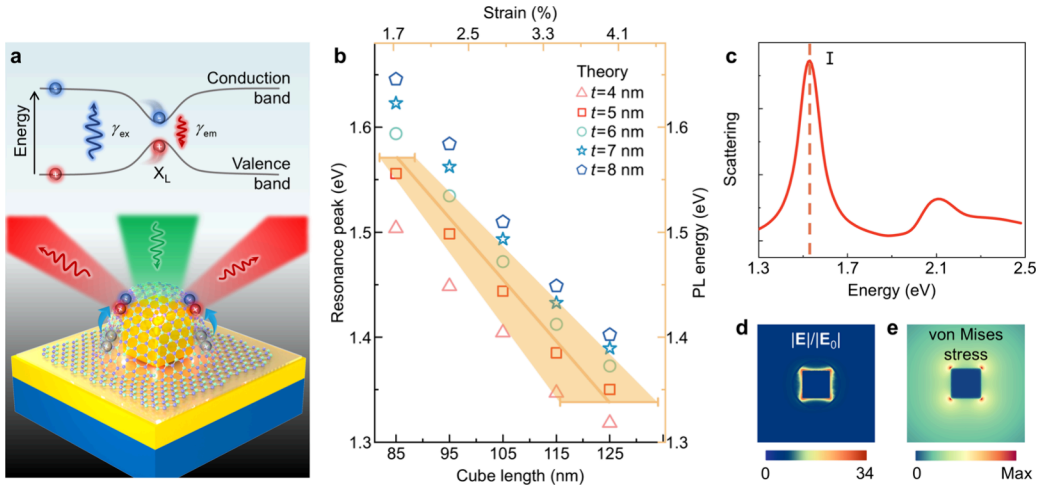

Figure 1. Mechanism for resonance tuning of localized exciton emission from a WSe_2 monolayer. (a) Schematic of the generation of localized excitons in a WSe_2-capped nanocavity. The nanocavity consists of an Au nanocube separated from an Au film by an Al_2O_3 gap layer. The energy diagram illustrates exciton localization within a potential well induced by local strain from the nanocube. (b) Alignment of plasmonic resonances with localized exciton energy at different edge lengths by varying the gap layer thicknesses. (c) Simulated scattering spectra of a nanocavity with an edge length of 95 nm and a gap thickness of 6 nm, showing spectral matching of cavity mode I with the localized exciton energy. (d and e) Electric field enhancement (d) and local strain distributions (e) at the top surface of the nanocube.

energy spectrum. To enable robust room temperature operations, particularly against thermal fluctuations, it is imperative to further red-shift the localized exciton, which, however, remains a great challenge. The difficulty lies in concurrently aligning strain-induced potential tuning and plasmonic resonance, resulting in the emission either being obscured by the overwhelming free exciton peak or remaining weak and undetectable when off-resonance with the plasmonic mode.

Here, we demonstrate broadband energy tuning of localized exciton emission from monolayer WSe_2 at room temperature. We utilize plasmonic cavities with an Au nanocube-on-mirror (NCoM) configuration as a monolithic integration of strain engineering and Purcell-enhanced spontaneous emission rate. Our design is driven by three key considerations: (1) The well-defined nanocube shape induces a local strain on WSe_2, creating a size-dependent potential that localizes the exciton. The energy of this localized exciton can be predicted based on an empirical correlation between the exciton energy shift and strain. (2) The plasmonic mode of the NCoM nanocavity is highly sensitive to its gap layer thickness. This extra-freedom allows for fine-tuning the cavity resonance to spectrally match the predicted energy of the localized exciton, resulting in Purcell-enhanced emission. (3) By adjusting both the nanocube length and gap thickness, we can simultaneously scan and enhance localized exciton emission across a record-large energy range, which is over 70 meV larger than that of existing approaches. Moreover, compared to bare nanoparticles, NCoM nanocavities exhibit up to 22-fold enhancement in localized exciton emission.

RESULTS AND DISCUSSION

The formation and enhancement of localized excitons are schematically illustrated in Figure 1a. The sharp corners of the Au NCoM nanocavity induce strain in WSe_2 through lattice deformation. This strain locally modifies the energy landscape, creating nanoscale potential wells that trap excitons, as depicted in the energy diagram of Figure 1a. The strain ε_{st} and the corresponding energy shift ΔE can be readily tuned by varying the edge length l of the nanocube, allowing control over the localized exciton emission energy E_L, which follows the empirical relation:[26]

$$E_L = E_{L0} + \Delta E \tag{1}$$

where E_{L0} = 1.57 eV is the localized exciton energy at ε_{st0} = 1.74%. The energy shift $\Delta E = \alpha(\varepsilon_{st} - \varepsilon_{st0})$ represents strain-dependent modulation of exciton energy, with α = −0.103 eV/%.[29] The orange solid line in Figure 1b presents the localized exciton energy as a function of strain, predicted from eq 1. The shaded region indicates the uncertainty in the exciton-strain relationship, determined from atomic force microscopy (AFM) measurements (Figure S1). Raman spectroscopy measurements further confirm that the strain in monolayer WSe_2 can be effectively tuned by tuning the nanocube edge length (Figure S2).

The plasmonic resonance of the nanocavity can be precisely tuned through the gap layer thickness t. For instance, the horizontal electric dipole of the nanocube interacts with its image charges in the Au film to form cavity mode I, whose energy E_{NC} depends on t according to a circuit model:[30−32]

$$E_{NC} = E_p(2\varepsilon_m + \varepsilon_\infty + 4\varepsilon_m\eta)^{-1/2} \tag{2}$$

where E_p denotes the plasmon energy of Au, ε_m and ε_∞ represent the permittivities of the dielectric medium and the corresponding background, respectively. The capacitance ratio, defined as $\eta = C_g/C_{NP}$, quantifies the normalized capacitance of the nanocavity ($C_g = \varepsilon_m\varepsilon_g^a A/t$) with respect to that of the nanocube ($C_{NP} = b\varepsilon_m\pi R$). Here, A is the effective area associated with the net charge distribution of mode I, ε_g = 2.4 represents the permittivity of Al_2O_3, and R is the equivalent radius representing the net charge area of the bottom surface of the nanocube (Figure S3). In this context, the gap thickness can be optimized by changing the edge length to align mode I with the localized exciton energy, as shown in Figure 1b. For example, in a nanocavity with l = 95 nm, setting the gap thickness t to 6 nm results in a simulated scattering spectrum where mode I closely overlaps with the exciton energy (Figure 1c). Notably, mode I exhibits a 34-fold field enhancement at

https://doi.org/10.1021/acsnano.5c21481
ACS Nano 2026, 20, 6279−6286

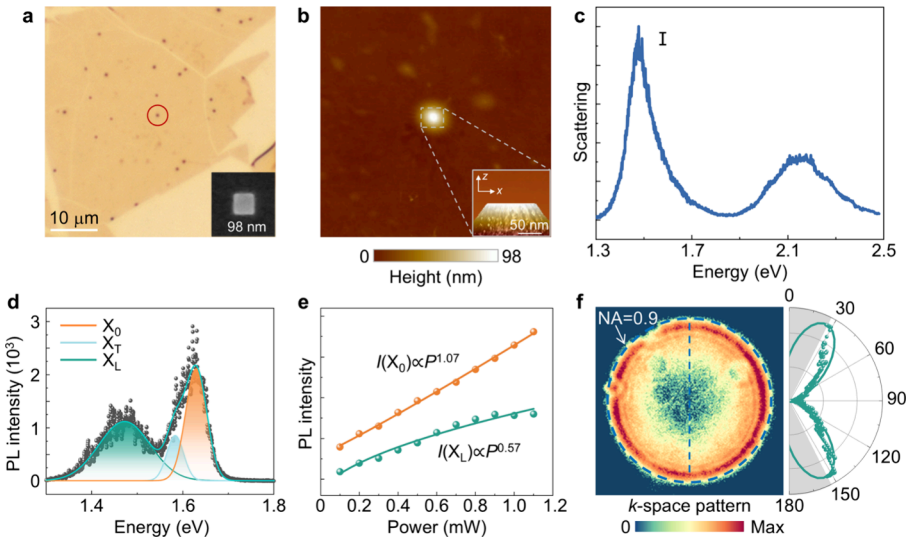

Figure 2. Realization of localized exciton emission in a WSe_2-capped nanocavity. (a) Optical microscope image of the hybrid structure. The inset shows the SEM image of the target structure. (b) AFM topography image of monolayer WSe_2 on the nanocavity highlighted as the red circle in (a). The inset shows a side-view AFM profile of the hybrid structure. (c) Scattering spectrum measured from the individual hybrid structure shown in (a). (d) PL spectrum of the WSe_2-capped nanocavity [red circle in (a)], with emission peaks for neutral exciton (X_0), trion (X_T), and localized exciton (X_L) identified through Gaussian fitting. (e) Power-dependent emission peak intensity of neutral excitons and localized excitons, showing the power saturation behavior of localized excitons. (f) Back focal plane image of localized exciton emission (left) and its corresponding polar emission pattern (right). The dots and line in right panel are for the experiment and simulation results, respectively.

the top corners of the nanocube (Figure 1d), which coincides with regions of maximum local strain (Figure 1e).

To validate our prediction, we fabricate the WSe_2-capped Au NCoM nanocavity using a bottom-up approach (see Methods). As shown in Figure 2a, the optical and scanning electron microscope (SEM) images reveal that the target nanocavity covered by monolayer WSe_2 has an edge length of 98 nm. Figure 2b presents the morphology of the WSe_2 monolayer within the labeled region in Figure 2a, as measured by AFM. It reveals that the WSe_2 is intact without punctures and conforms closely to the top surface of the nanocube, forming sharp curvatures at the nanocube top corners. According to Hencky's model,[33,34] the AFM-measured deformation induces a strain of 2.68%, leading to a reduction in the optical bandgap to 1.48 eV. To ensure alignment between the plasmonic resonance and the localized exciton emission energy, the gap layer thickness is set to 6 nm, following the design framework in Figure 1b. The plasmonic response of the designed nanocavity is resolved through side-illumination scattering spectroscopy, revealing a pronounced cavity mode (mode I) that overlaps with the localized exciton energy to accelerate the emission rate (Figure 2c).

In Figure 2d, we present the photoluminescence (PL) spectrum measured from the selected nanocavity (Figure 2a) under 532 nm excitation at room temperature. In contrast to unstrained WSe_2 (Figure S4), a distinct low-energy PL peak emerges at 1.48 eV. Under identical experimental conditions, the NCoM nanocavities and bare nanocubes without WSe_2 coverage exhibit no detectable plasmonic scattering-related signal (Figures S5 and S6). Thus, the low-energy peak in the PL spectra of the WSe_2-capped structures can be unambiguously attributed to localized exciton emission, with no contribution from plasmonic scattering or the intrinsic PL of the NCoM nanocavity. This assignment is further supported by the temperature-dependent PL measurements (Figure S7), whose spectral evolution closely follows the characteristic behavior of localized excitons.[18] For a clear comparison, the PL spectra are fitted with Gaussian functions. The high-energy peak originates from overlapping emissions of the neutral exciton (X_0) at ~1.63 eV and a trion (X_T) at ~1.59 eV.[35] The low-energy peak, characterized by a broad line width and a large energy separation from the X_0 peak, is distinct from other excitonic complexes (e.g., trion, dark exciton, biexciton). This allows us to identify it as the localized exciton (X_L) emission, consistent with previous reports.[25,36] Furthermore, comparative PL spectra acquired from the nanocube site and its surrounding regions reveal that the X_L feature is exclusively present in the strained region directly atop the nanocube (Figure S8). This strong spatial confinement indicates that the X_L feature arises from strain-induced exciton localization, rather than from intrinsic point defects or wrinkle-induced inhomogeneities, which are typically distributed more broadly across the monolayer.[4,6]

To further confirm the X_L emission, we examine the power-dependent evolution of X_0 and X_L emissions in Figure 2e. The emissions are fitted with power laws, revealing a linear and sublinear power dependence for X_0 and X_L on pump intensity, respectively. This saturating behavior is a clear hallmark of X_L emission, which is typically associated with defect states residing in trap potentials and tends to saturate at lower excitation powers compared to free excitons.[37] The back focal plane (BFP) imaging technique is employed to resolve the angular emission pattern of localized excitons, as shown in Figure 2f. The BFP image reveals a doughnut-shaped far-field distribution (left panel of Figure 2f), which is also observed in the X_L emission from the WSe_2-capped bare nanocube (Figure S9). Notably, the BFP image of X_L is clearly distinct from the balloon-shaped scattering pattern of the nanocavity mode I (Figure S10), demonstrating that the doughnut-shaped far-field emission is an intrinsic property of X_L. Numerical simulations further support the doughnut-shaped emission feature of X_L, as evidenced by the polar plot in the right panel

https://doi.org/10.1021/acsnano.5c21481
ACS Nano 2026, 20, 6279−6286

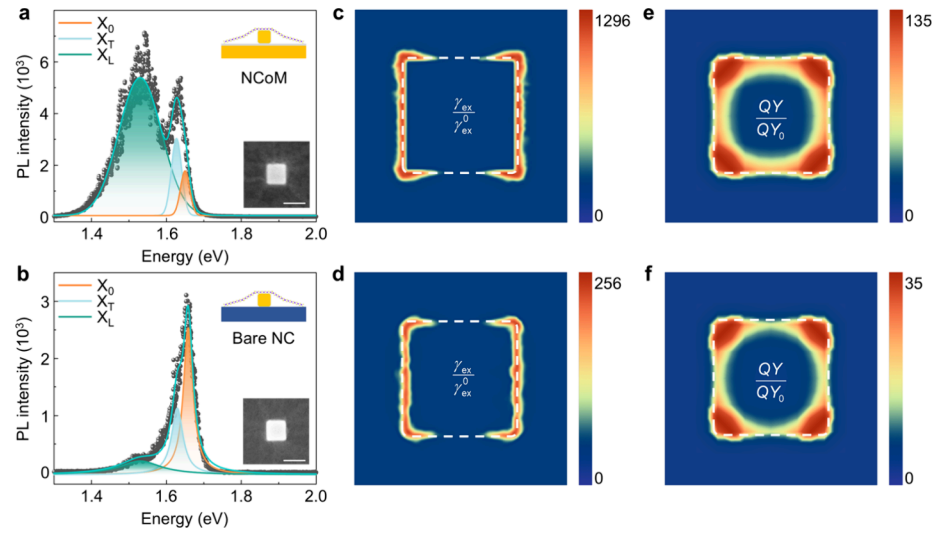

Figure 3. Plasmon-enhanced localized exciton emission from a WSe_2 monolayer. (a and b) PL spectra from the WSe_2-capped nanocavity (a) and WSe_2-capped bare nanocube (b). The upper and lower insets show the geometry and SEM images of two plasmonic systems, respectively. The scale bar is 100 nm. (c and d) Simulated excitation rate enhancement distributions for localized excitons in the nanocavity (c) and bare nanocube (d). (e and f) Simulated quantum yield enhancement maps for localized excitons in the nanocavity (e) and bare nanocube (f).

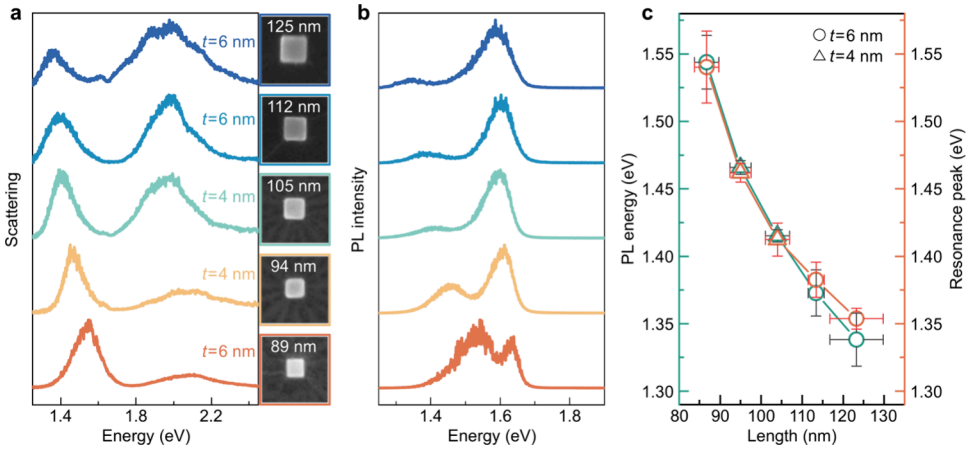

Figure 4. Resonant red-shifting of localized exciton energy using a nanocavity. (a and b) Normalized scattering (a) and PL spectra (b) of WSe_2-capped nanocavities with varying edge lengths. The SEM images show nanocavities with edge lengths ranging from 89 to 125 nm. The gap layer thickness (t) in each cavity is adjusted to spectrally align cavity mode I with the localized exciton energy. (c) Energies of localized excitons and cavity mode I as a function of the edge length. Green and orange hollow dots represent the exciton and mode I energies, respectively.

of Figure 2f. This behavior contrasts sharply with that of free excitons, which exhibit an in-plane (IP) dipole with maximum intensity along the surface normal (Figure S11). The observed difference can be attributed to the strain distribution shown in Figure 1e, where the highest strain occurs at the periphery of the top corners of the nanocube. At these locations, the deformation of WSe_2 induces a transition of the exciton from an IP dipole to a tilted configuration, consistent with recent findings on X_L characteristics.[38,39]

To gain deeper insights into the enhanced emission of X_L, we conducted the PL measurements on the monolayer WSe_2 integrated with a nanocavity and on a control sample deposited on a nanocube atop a SiO_2 substrate, as shown in Figure 3a,b. For a fair comparison, nanocubes of identical dimensions (l = 89 nm) are used to ensure equivalent deformation (Figure S12) and consistent strain distribution on the WSe_2 monolayer. To ensure a consistent comparison, we constrained identical line widths for X_0, X_T, and X_L when fitting the spectra of the WSe_2-capped nanocavity and the WSe_2-capped bare nanocube of the same size. When coupled with the nanocavity, the X_L emission peak is significantly intensified, in stark contrast to the shallow shoulder observed in the control sample. This results in a 22-fold enhancement in X_L emission relative to the control.

We further employ full-wave simulation methods to analyze the enhancement of X_L emission. The enhancement factor for X_L emission relative to free space is given by[40]

$$EF(\mathbf{r}, \omega_{ex}, \omega_{em}) \propto \frac{\gamma_{ex}(\mathbf{r}, \omega_{ex})}{\gamma_{ex}^{0}(\mathbf{r}, \omega_{ex})} \frac{QY(\mathbf{r}, \omega_{em})}{QY_0(\mathbf{r}, \omega_{em})} \quad (3)$$

where γ_{ex} and QY represent excitation rate and quantum yield, respectively, in the presence of the plasmonic structures. The terms in the denominator correspond to these quantities in free space. At the excitation wavelength of 532 nm, the nanocavity supports a film-coupled quadrupole mode, while the bare nanocube sustains a conventional quadrupole mode (Figure S13). Both modes reshape the incident light field,

https://doi.org/10.1021/acsnano.5c21481
ACS Nano 2026, 20, 6279−6286

leading to a substantial enhancement of the out-of-plane (OP) local electric field. This is ideal for boosting the excitation rate, as this OP component shapes the field vector to match the tilted X_L and enhance their interaction. As a result, both plasmonic systems achieve an over two-orders-of-magnitude increase in the excitation rate at the nanocube corners, with the NCoM nanocavity providing a markedly stronger enhancement than the bare nanocube (Figure 3c,d). This distinction is further supported by the comparative Raman enhancements measured for the two structures (Figure S14). The mode I reveals out-of-plane field enhancement at the top corners of the nanocavity (Figure S15), which contributes to the local density of optical states and enhances localized exciton emission through the Purcell effect. It is important to note that the out-of-plane field enhancement serves as a passive photonic environment that accelerates the emitter's radiation rate, rather than the gold itself acting as the primary emitter. This leads to a nearly 4-fold increase in quantum yield (Figure 3e) compared to the bare nanocube (Figure 3f), whose dipole mode is largely nonresonant with the X_L emission (Figure S13). Consequently, the theoretical PL enhancement factor for the nanocavity is 20-fold greater than that of the bare nanocube, in excellent agreement with experimental measurements. This further confirms that, in contrast to conventional plasmonic nanoparticles, the nanocavity offers an additional degree of freedom for simultaneously controlling the excitation and emission of X_L.

The chemically synthesized Au nanocubes exhibit a size distribution ranging from 80 to 130 nm (Figure S16), thereby enabling the tuning of the X_L emission over a broad energy range. By leveraging spectroscopy-assisted nanomanipulation, we deterministically select nanocubes with predefined edge lengths to apply controlled strain on the WSe_2 monolayer. Following the framework illustrated in Figure 1b, we precisely control the deposition of the gap layer to construct nanocavities, in which mode I aligns with the theoretically predicted energies of localized excitons. This can be evident from scattering spectra of nanocavities in Figure 4a, where mode I redshifts with l increasing, consistent with the strain-dependent energy shift of the X_L emission (Figure 1b). Further fine-tuning of the gap enables optimized plasmon-localized exciton interactions through spectral matching, facilitating on-demand excitation of the X_L peak across all five nanocavities, as clearly demonstrated by the PL spectra in Figure 4b.

When the nanocube edge length l exceeds 125 nm, the monolayer WSe_2 transferred onto the nanocube can no longer sustain the induced strain and consequently ruptures (Figure S17). By varying l, we achieve a tunable energy shift from 1.590 to 1.343 eV (Figure S18), approaching the strain-induced redshift limit of 247 meV, as summarized in Table S1. In parallel, both X_0 and X_T emissions exhibit systematic redshifts with increasing strain (Figure S19), which is consistent with previously reported strain-dependent free exciton emissions in TMD monolayers.[29] Figure 4c illustrates the dependence of X_L and mode I energies on the nanocube edge length l, revealing their strong spectral alignment across the range of l. Consequently, compared to bare nanocubes (Figure S20), the nanocavity yield significantly more prominent X_L peaks, with up to a 22-fold enhancement in emission intensity. These results underscore the ability of the nanocavity platform to precisely control plasmon-exciton coupling, offering a powerful approach for tailoring localized excitonic emission in strained monolayer semiconductors.

CONCLUSIONS

In conclusion, we have demonstrated the room-temperature resonance tuning of localized exciton emission in a WSe_2 monolayer using a plasmonic nanocavity. A general model is developed, utilizing tunable plasmonic modes to enhance localized exciton emission intensity upon red-shifting, enabling precise control over exciton−plasmon interactions. This leads to up to a 22-fold enhancement in emission from the WSe_2-capped nanocavity, allowing access to the upper limit of the red-shifted localized exciton, which is typically masked by the neutral exciton background. Our work establishes a robust strategy for on-demand tuning of the localized excitonic states, providing a solid foundation for scalable, high-brightness, and wavelength-customizable nonclassical light sources. Such advancements could drive the development of on-chip quantum photonic circuits, quantum emitters, and tunable single-photon devices for quantum information processing and communication.

METHODS

Sample Preparation

The WSe_2-capped NCoM nanocavity was fabricated via a bottom-up approach. First, an ultrasmooth 50 nm-thick Au film was prepared using a template-stripping method. A thin Al_2O_3 spacer layer was then deposited by atomic layer deposition at 150 °C. To fabricate the plasmonic nanocavity, a solution of Au nanocubes wrapped with a 2 nm cetyltrimethylammonium bromide (CTAB) shell (Nanoseedz, Inc. and MeLab, Inc.) was diluted with deionized water at a 1:6 volume ratio and spin-coated onto the Al_2O_3 layer. Finally, a monolayer of WSe_2, grown by chemical vapor deposition, was transferred onto the Au nanocubes using a dry-transfer technique, forming the WSe_2-capped NCoM hybrid structure.

Optical Measurements

Scattering spectra were measured using a custom-built confocal darkfield microscopy system.[41,42] P-polarized white light from a halogen lamp was directed onto the sample at an incident angle of 70° through a 50× Mitutoyo objective (NA = 0.55). The scattered light was collected by an upright 50× Nikon objective (NA = 0.4), spatially filtered via a pinhole, and coupled into a spectrometer (Andor Shamrock SR-303IB) equipped with an air-cooled CCD camera. For room-temperature PL measurements, the sample was excited using a 532 nm continuous-wave laser focused through a 150× Leica objective (NA = 0.9). The PL emission was collected by the same objective filtered with a 532 nm long-pass filter, and directed into a spectrometer (Andor Shamrock SR-500i). The laser spot diameter at the sample plane was ∼1 μm. To measure the far-field emission pattern of the hybrid nanocavity, a 4f correlator system (see Figure S21) was employed to image the back focal plane of the objective onto an sCMOS camera (Dhyana 400BSI V3, Tucsen Inc.).

Numerical Calculation

The plasmonic responses of the NCoM were simulated using the finite element method (COMSOL Multiphysics). The nanocube dimensions were set to match the experimental conditions. The dielectric constants of monolayer WSe_2 and Au were taken from experimental data by Johnson and Christy,[43] while those of Al_2O_3 and CTAB were fixed at 1.5. The scattering spectra were computed using a two-step procedure. First, periodic boundary conditions were applied, and a linearly polarized plane wave at an incident angle of 70° was used as the excitation source to generate the background field in the absence of the nanoparticle. Second, the scattered field was collected over a solid angle corresponding to a numerical aperture of 47.2°, consistent with that of the objective lens, to obtain the scattering spectra. Localized excitons were modeled as point dipoles, and the corresponding PL far-field pattern was obtained by placing dipole emitters oriented along the tangent directions at the top

https://doi.org/10.1021/acsnano.5c21481
ACS Nano 2026, 20, 6279−6286

corners of the nanocube (see Figure S22). The quantum yield of WSe_2 coupled to the nanocavity was calculated using the dyadic Green's function within a three-dimensional finite-difference time-domain (FDTD) method.[44,45] The enhanced spontaneous emission rate, $\gamma_r = \gamma_{rad}/\gamma_{rad0}$, was evaluated by performing raster scans of an point dipole emitter on a 15 × 15 grid positioned above the nanocube. The enhanced quantum yield was then determined using the equation:

$$QY = \frac{\gamma_r}{\gamma_r + \gamma_{nr} + (1 - Q_0)/Q_0} \quad (4)$$

where Q_0 = 1.5% is the intrinsic quantum yield of the monolayer WSe_2.[17]

Strain Calculation

To investigate the origin of the localized exciton emission in the WSe_2-capped NCoM nanocavity, we calculated the local strain distribution in the WSe_2 membrane across the nanocube using the Hencky's model:[33,34]

$$\varepsilon_{st} = \frac{A_0(\nu)(1-\nu)K(\nu)^{2/3}}{4}\left(\frac{h}{R}\right)^2 \quad (5)$$

where ν is the Poisson's ratio of the membrane, $A_0(\nu)$ and $K(\nu)$ are numerical parameters determined by ν, which can be obtained from Hencky's solution. The membrane height (h) and radius (R) were extracted from AFM topography measurements. For WSe_2, we adopted ν = 0.19,[46] with $A_0(\nu)$ = 1.66 and $K(\nu)$ = 3.2.

ASSOCIATED CONTENT

Supporting Information

The Supporting Information is available free of charge at https://pubs.acs.org/doi/10.1021/acsnano.5c21481.

Deformation statistics in monolayer WSe_2; Raman spectra of WSe_2-capped nanocavities; comparison of the circuit model with simulated data for cavity mode; PL spectrum of unstrained monolayer WSe_2; PL and scattering measurements of nanocavity structures with varying sizes; PL and scattering measurements of nanocube structures with varying sizes; temperature-dependent PL emissions of localized excitons; PL spectra acquired from the strained and unstrained regions of monolayer WSe_2; localized exciton emission from the WSe_2-capped bare nanocube; far-field patterns measured using back-focal-plane imaging; far-field emission patterns of the neutral excitons in monolayer WSe_2; deformation in the monolayer WSe_2 capped on a nanocavity and a bare nanocube; plasmonic responses of a nanocavity and a bare nanocube covered with a monolayer WSe_2; Raman enhancement of WSe_2-capped nanocavities and WSe_2-capped bare nanocubes; side-view electric-field enhancement maps of the nanocavity mode I; size distribution of Au nanocubes determined from SEM images; AFM topography of monolayer WSe_2 on nanocavities with edge lengths ranging from 89 to 150 nm; minimum and maximum energy shift for local exciton under resonance tuning; strain response of free excitons; localized exciton energy shifts in WSe_2-capped bare nanocubes; optical setup for PL spectrum and BFP imaging; and far-field emission patterns of localized exciton (PDF)

AUTHOR INFORMATION

Corresponding Authors

Chaojie Ma − *Beijing National Laboratory for Condensed Matter Physics, Institute of Physics, Chinese Academy of Sciences, Beijing 100190, China;* orcid.org/0000-0003-3649-5220; Email: chaojiema@iphy.ac.cn

Kaihui Liu − *State Key Laboratory for Mesoscopic Physics, Frontiers Science Center for Nanooptoelectronics, School of Physics, Peking University, Beijing 100871, China;* orcid.org/0000-0002-8781-2495; Email: khliu@pku.edu.cn

Fajun Xiao − *Key Laboratory of Light-Field Manipulation and Information Acquisition, Ministry of Industry and Information Technology, and Shaanxi Key Laboratory of Optical Information Technology, School of Physical Science and Technology, Northwestern Polytechnical University, Xi'an 710129, China;* orcid.org/0000-0002-7656-7869; Email: fjxiao@nwpu.edu.cn

Authors

Qifa Wang − *Key Laboratory of Light-Field Manipulation and Information Acquisition, Ministry of Industry and Information Technology, and Shaanxi Key Laboratory of Optical Information Technology, School of Physical Science and Technology, Northwestern Polytechnical University, Xi'an 710129, China;* orcid.org/0000-0001-8561-3962

Guodong Xue − *State Key Laboratory for Mesoscopic Physics, Frontiers Science Center for Nanooptoelectronics, School of Physics, Peking University, Beijing 100871, China*

Cheng Ji − *Key Laboratory of Light-Field Manipulation and Information Acquisition, Ministry of Industry and Information Technology, and Shaanxi Key Laboratory of Optical Information Technology, School of Physical Science and Technology, Northwestern Polytechnical University, Xi'an 710129, China*

Yuxin Li − *Key Laboratory of Light-Field Manipulation and Information Acquisition, Ministry of Industry and Information Technology, and Shaanxi Key Laboratory of Optical Information Technology, School of Physical Science and Technology, Northwestern Polytechnical University, Xi'an 710129, China*

Chenyang Li − *Key Laboratory of Light-Field Manipulation and Information Acquisition, Ministry of Industry and Information Technology, and Shaanxi Key Laboratory of Optical Information Technology, School of Physical Science and Technology, Northwestern Polytechnical University, Xi'an 710129, China*

Liping Hou − *Key Laboratory of Light-Field Manipulation and Information Acquisition, Ministry of Industry and Information Technology, and Shaanxi Key Laboratory of Optical Information Technology, School of Physical Science and Technology, Northwestern Polytechnical University, Xi'an 710129, China*

Xiaobing Zheng − *Key Laboratory of Light-Field Manipulation and Information Acquisition, Ministry of Industry and Information Technology, and Shaanxi Key Laboratory of Optical Information Technology, School of Physical Science and Technology, Northwestern Polytechnical University, Xi'an 710129, China*

Qinghong Yu − *Key Laboratory of Light-Field Manipulation and Information Acquisition, Ministry of Industry and Information Technology, and Shaanxi Key Laboratory of*

https://doi.org/10.1021/acsnano.5c21481
ACS Nano 2026, 20, 6279−6286

Optical Information Technology, School of Physical Science and Technology, Northwestern Polytechnical University, Xi'an 710129, China

Xuetao Gan − *Key Laboratory of Light-Field Manipulation and Information Acquisition, Ministry of Industry and Information Technology, and Shaanxi Key Laboratory of Optical Information Technology, School of Physical Science and Technology, Northwestern Polytechnical University, Xi'an 710129, China;* orcid.org/0000-0003-2469-5807

Jianlin Zhao − *Key Laboratory of Light-Field Manipulation and Information Acquisition, Ministry of Industry and Information Technology, and Shaanxi Key Laboratory of Optical Information Technology, School of Physical Science and Technology, Northwestern Polytechnical University, Xi'an 710129, China*

Complete contact information is available at: https://pubs.acs.org/10.1021/acsnano.5c21481

Author Contributions

Q.W. and G.X. contributed equally to this work. F.X. and Q.W. conceived the experiments and developed the theory. Q.W. performed the experiments, gathered the data, and developed the numerical simulations. G.X. performed the growth experiments. C.J., Y.L., X.Z., and Q.Y. assisted in the sample characterizations. C.L. and L.H. contributed to the numerical simulations. X.G. and J.Z. suggested the optical measurements. F.X., C.M., and K.L. supervised the project. All of the authors discussed the results and wrote the manuscript.

Notes

The authors declare no competing financial interest.

■ ACKNOWLEDGMENTS

This work was supported by the National Key R&D Program of China (2022YFA1404800), the National Natural Science Foundation of China (NSFC) (12274345 and 52025023), the Natural Science Basic Research Plan in Shaanxi Province (2024JC-JCQN-08), and the Innovation Foundation for Doctor Dissertation of Northwestern Polytechnical University (CX2022078). The authors would like to thank Dr. C. Zhao at the Analytical & Testing Center of Northwestern Polytechnical University for assistance with AFM measurements.

■ REFERENCES

(1) Gu, J.; Chakraborty, B.; Khatoniar, M.; Menon, V. M. A room-temperature polariton light-emitting diode based on monolayer WS_2. *Nat. Nanotechnol.* **2019**, *14*, 1024−1028.

(2) Tsai, H.; Nie, W.; Blancon, J.-C.; Toumpos, C. C. S.; Asadpour, R.; Harutyunyan, B.; Neukirch, A. J.; Verduzco, R.; Crochet, J. J.; Tretiak, S.; Pedesseau, L.; Even, J.; Alam, M. A.; Gupta, G.; Lou, J.; Ajayan, P. M.; Bedzyk, M. J.; Kanatzidis, M. G.; Mohite, A. D. High-efficiency two-dimensional Ruddlesden-Popper perovskite solar cells. *Nature* **2016**, *536*, 312−316.

(3) Dufferwiel, S.; Lyons, T. P.; Solnyshkov, D. D.; Trichet, A. A. P.; Withers, F.; Schwarz, S.; Malpuech, G.; Smith, J. M.; Novoselov, K. S.; Skolnick, M. S.; Krizhanovskii, D. N.; Tartakovskii, A. I. Valley-addressable polaritons in atomically thin semiconductors. *Nat. Photonics* **2017**, *11*, 497−501.

(4) Linhart, L.; Paur, M.; Smejkal, V.; Burgdoerfer, J.; Mueller, T.; Libisch, F. Localized intervalley defect excitons as single-photon emitters in WSe_2. *Phys. Rev. Lett.* **2019**, *123*, No. 146401.

(5) Qi, P.; Luo, Y.; Shi, B.; Li, W.; Liu, D.; Zheng, L.; Liu, Z.; Hou, Y.; Fang, Z. Phonon scattering and exciton localization: molding exciton flux in two dimensional disorder energy landscape. *eLight* **2021**, *1*, 6.

(6) Yanev, E. S.; Darlington, T. P.; Ladyzhets, S. A.; Strasbourg, M. C.; Trovatello, C.; Liu, S.; Rhodes, D. A.; Hall, K.; Sinha, A.; Borys, N. J.; Hone, J. C.; Schuck, P. J. Programmable nanowrinkle-induced room-temperature exciton localization in monolayer WSe_2. *Nat. Commun.* **2024**, *15*, 1543.

(7) Abramov, A. N.; Chestnov, I. Y.; Alimova, E. S.; Ivanova, T.; Mukhin, I. S.; Krizhanovskii, D. N.; Shelykh, I. A.; Iorsh, I. V.; Kravtsov, V. Photoluminescence imaging of single photon emitters within nanoscale strain profiles in monolayer WSe_2. *Nat. Commun.* **2023**, *14*, 5737.

(8) Chen, S.; Wang, C.; Cai, H.; Ma, L.; Qu, Y.; Liu, Z.; Wang, S.; Zhan, J.; Tan, Q.; Sheng, B.; Liu, X.; Wang, X.; Zhang, X.; Xu, J.; Gao, W.; Liu, Q. Realization of single-photon emitters with high brightness and high stability and excellent monochromaticity. *Matter* **2024**, *7*, 1106−1116.

(9) Moody, G.; Tran, K.; Lu, X.; Autry, T.; Fraser, J. M.; Mirin, R. P.; Yang, L.; Li, X.; Silverman, K. L. Microsecond valley lifetime of defect-bound excitons in monolayer WSe_2. *Phys. Rev. Lett.* **2018**, *121*, No. 057403.

(10) Li, X.; Jones, A. C.; Choi, J.; Zhao, H.; Chandrasekaran, V.; Pettes, M. T.; Piryatinski, A.; Tschudin, M. A.; Reiser, P.; Broadway, D. A.; Maletinsky, P.; Sinitsyn, N.; Crooker, S. A.; Htoon, H. Proximity-induced chiral quantum light generation in strain-engineered $WSe_2/NiPS_3$ heterostructures. *Nat. Mater.* **2023**, *22*, 1311−1316.

(11) Lee, S.-J.; So, J.-P.; Kim, R. M.; Kim, K.-H.; Rha, H.-H.; Na, G.; Han, J. H.; Jeong, K.-Y.; Nam, K. T.; Park, H.-G. Spin angular momentum-encoded single-photon emitters in a chiral nanoparticle-coupled WSe_2 monolayer. *Sci. Adv.* **2024**, *10*, No. eadn7210.

(12) Wang, Q.; Maisch, J.; Tang, F.; Zhao, D.; Yang, S.; Joos, R.; Portalupi, S. L.; Michler, P.; Smet, J. H. Highly polarized single photons from strain-induced quasi-1D localized excitons in WSe_2. *Nano Lett.* **2021**, *21*, 7175−7182.

(13) Paralikis, A.; Piccinini, C.; Madigawa, A. A.; Metuh, P.; Vannucci, L.; Gregersen, N.; Munkhbat, B. Tailoring polarization in WSe_2 quantum emitters through deterministic strain engineering. *npj 2D Mater. Appl.* **2024**, *8*, 59.

(14) So, J.-P.; Kim, H.-R.; Baek, H.; Jeong, K.-Y.; Lee, H.-C.; Huh, W.; Kim, Y. S.; Watanabe, K.; Taniguchi, T.; Kim, J.; Lee, C.-H.; Park, H.-G. Electrically driven strain-induced deterministic single-photon emitters in a van der Waals heterostructure. *Sci. Adv.* **2021**, *7*, No. eabj3176.

(15) Lopez, P. H.; Heeg, S.; Schattauer, C.; Kovalchuk, S.; Kumar, A.; Bock, D. J.; Kirchhof, J. N.; Hoefer, B.; Greben, K.; Yagodkin, D.; Linhart, L.; Libisch, F.; Bolotin, K. I. Strain control of hybridization between dark and localized excitons in a 2D semiconductor. *Nat. Commun.* **2022**, *13*, 7691.

(16) He, Y.-M.; Clark, G.; Schaibley, J. R.; He, Y.; Chen, M.-C.; Wei, Y.-J.; Ding, X.; Zhang, Q.; Yao, W.; Xu, X.; Lu, C.-Y.; Pan, J.-W. Single quantum emitters in monolayer semiconductors. *Nat. Nanotechnol.* **2015**, *10*, 497−502.

(17) Luo, Y.; Shepard, G. D.; Ardelean, J. V.; Rhodes, D. A.; Kim, B.; Barmak, K.; Hone, J. C.; Strauf, S. Deterministic coupling of site-controlled quantum emitters in monolayer WSe_2 to plasmonic nanocavities. *Nat. Nanotechnol.* **2018**, *13*, 1137−1142.

(18) Li, S.; Chui, K. K.; Shen, F.; Huang, H.; Wen, S.; Yam, C.; Shao, L.; Xu, J.; Wang, J. Generation and detection of strain-localized excitons in WS_2 monolayer by plasmonic metal nanocrystals. *ACS Nano* **2022**, *16*, 10647−10656.

(19) Xu, D. D.; Vong, A. F.; Utama, M. I. B.; Lebedev, D.; Ananth, R.; Hersam, M. C.; Weiss, E. A.; Mirkin, C. A. Sub-diffraction correlation of quantum emitters and local strain fields in strain-engineered WSe_2 monolayers. *Adv. Mater.* **2024**, *36*, No. 2314242.

(20) Xu, D. D.; Vong, A. F.; Lebedev, D.; Ananth, R.; Wong, A. M.; Brown, P. T.; Hersam, M. C.; Mirkin, C. A.; Weiss, E. A. Conversion of classical light emission from a nanoparticle-strained WSe_2

monolayer into quantum light emission via electron beam irradiation. *Adv. Mater.* **2023**, *35*, No. 2208066.
(21) Peng, L.; Chan, H.; Choo, P.; Odom, T. W.; Sankaranarayanan, S. K. R. S.; Ma, X. Creation of single-photon emitters in WSe_2 monolayers using nanometer-sized gold tips. *Nano Lett.* **2020**, *20*, 5866−5872.
(22) Branny, A.; Kumar, S.; Proux, R.; Gerardot, B. D. Deterministic strain-induced arrays of quantum emitters in a two-dimensional semiconductor. *Nat. Commun.* **2017**, *8*, No. 15053.
(23) Palacios-Berraquero, C.; Kara, D. M.; Montblanch, A. R. P.; Barbone, M.; Latawiec, P.; Yoon, D.; Ott, A. K.; Loncar, M.; Ferrari, A. C.; Atature, M. Large-scale quantum-emitter arrays in atomically thin semiconductors. *Nat. Commun.* **2017**, *8*, No. 15093.
(24) Parto, K.; Azzam, S. I.; Banerjee, K.; Moody, G. Defect and strain engineering of monolayer WSe_2 enables site-controlled single-photon emission up to 150K. *Nat. Commun.* **2021**, *12*, 3585.
(25) Lee, H.; Kim, I.; Park, C.; Kang, M.; Choi, J.; Jeong, K.-Y.; Mun, J.; Kim, Y.; Park, J.; Raschke, M. B.; Park, H.-G.; Jeong, M. S.; Rho, J.; Park, K.-D. Inducing and probing localized excitons in atomically thin semiconductors via tip-enhanced cavity-spectroscopy. *Adv. Funct. Mater.* **2021**, *31*, No. 2102893.
(26) Koo, Y.; Kim, Y.; Choi, S. H.; Lee, H.; Choi, J.; Lee, D. Y.; Kang, M.; Lee, H. S.; Kim, K. K.; Lee, G.; Park, K.-D. Tip-induced nano-engineering of strain, bandgap, and exciton funneling in 2D semiconductors. *Adv. Mater.* **2021**, *33*, No. 2008234.
(27) Kumar, S.; Kaczmarczyk, A.; Gerardot, B. D. Strain-induced spatial and spectral isolation of quantum emitters in mono- and bilayer WSe_2. *Nano Lett.* **2015**, *15*, 7567−7573.
(28) Li, Z.; Lv, Y.; Ren, L.; Li, J.; Kong, L.; Zeng, Y.; Tao, Q.; Wu, R.; Ma, H.; Zhao, B.; Wang, D.; Dang, W.; Chen, K.; Liao, L.; Duan, X.; Duan, X.; Liu, Y. Efficient strain modulation of 2D materials via polymer encapsulation. *Nat. Commun.* **2020**, *11*, 1151.
(29) Kumar, A. M.; Yagodkin, D.; Rosati, R.; Bock, D. J.; Schattauer, C.; Tobisch, S.; Hagel, J.; Hoefer, B.; Kirchhof, J. N.; Lopez, P. H.; Burfeindt, K.; Heeg, S.; Gahl, C.; Libisch, F.; Malic, E.; Bolotin, K. I. Strain fingerprinting of exciton valley character in 2D semiconductors. *Nat. Commun.* **2024**, *15*, 7546.
(30) Baumberg, J. J.; Aizpurua, J.; Mikkelsen, M. H.; Smith, D. R. Extreme nanophotonics from ultrathin metallic gaps. *Nat. Mater.* **2019**, *18*, 668−678.
(31) Benz, F.; de Nijs, B.; Tserkezis, C.; Chikkaraddy, R.; Sigle, D. O.; Pukenas, L.; Evans, S. D.; Aizpurua, J.; Baumberg, J. J. Generalized circuit model for coupled plasmonic systems. *Opt. Express* **2015**, *23*, 33255−33269.
(32) Wang, Q.; Li, C.; Hou, L.; Zhang, H.; Gan, X.; Liu, K.; Premaratne, M.; Xiao, F.; Zhao, J. Unveiling radial breathing mode in a particle-on-mirror plasmonic nanocavity. *Nanophotonics* **2022**, *11*, 487−494.
(33) Koenig, S. P.; Boddeti, N. G.; Dunn, M. L.; Bunch, J. S. Ultrastrong adhesion of graphene membranes. *Nat. Nanotechnol.* **2011**, *6*, 543−546.
(34) Lloyd, D.; Liu, X.; Christopher, J. W.; Cantley, L.; Wadehra, A.; Kim, B. L.; Goldberg, B. B.; Swan, A. K.; Bunch, J. S. Band gap engineering with ultralarge biaxial strains in suspended monolayer MoS_2. *Nano Lett.* **2016**, *16*, 5836−5841.
(35) Zhao, S.; Tao, L.; Miao, P.; Wang, X.; Liu, Z.; Wang, Y.; Li, B.; Sui, Y.; Wang, Y. Strong room-temperature emission from defect states in CVD-grown WSe_2 nanosheets. *Nano Res.* **2018**, *11*, 3922−3930.
(36) Yagodkin, D.; Greben, K.; Ascunce, A. E.; Kovalchuk, S.; Ghorbani-Asl, M.; Jain, M.; Kretschmer, S.; Severin, N.; Rabe, J. P.; Krasheninnikov, A. V.; Koch, C. T.; Bolotin, K. I. Extrinsic localized excitons in patterned 2D semiconductors. *Adv. Funct. Mater.* **2022**, *32*, No. 2203060.
(37) Schmidt, T.; Lischka, K.; Zulehner, W. Excitation-power dependence of the near-band-edge photoluminescence of semiconductors. *Phys. Rev. B* **1992**, *45*, 8989−8994.
(38) Luo, Y.; Liu, N.; Kim, B.; Hone, J.; Strauf, S. Exciton dipole orientation of strain-induced quantum emitters in WSe_2. *Nano Lett.* **2020**, *20*, 5119−5126.
(39) Jeong, H.; Suh, H. C.; Cho, G. H.; Joo, H.; Koo, Y.; Ko, H.; Kim, K. K.; Kim, Y.; Kim, J.; Park, K.-D.; Jeong, M. S. Large-area bright emission of plasmon-coupled dark excitons at room temperature. *Adv. Sci.* **2025**, *12*, No. 2411841.
(40) Akselrod, G. M.; Ming, T.; Argyropoulos, C.; Hoang, T. B.; Lin, Y.; Ling, X.; Smith, D. R.; Kong, J.; Mikkelsen, M. H. Leveraging nanocavity harmonics for control of optical processes in 2D semiconductors. *Nano Lett.* **2015**, *15*, 3578−3584.
(41) Wang, Q.; Hou, L.; Li, C.; Zhou, H.; Gan, X.; Liu, K.; Xiao, F.; Zhao, J. Toward high-performance refractive index sensor using single Au nanoplate-on-mirror nanocavity. *Nanoscale* **2022**, *14*, 10773−10779.
(42) Wang, Q.; Liu, J.; Li, C.; Hou, L.; Wang, P.; Gan, X.; Liu, K.; Lei, D.; Zhao, J.; Xiao, F. On-demand fabrication and manipulation of single plasmonic trimers for ultrasensitive enantiomer detection. *Adv. Funct. Mater.* **2025**, *35*, No. 2412985.
(43) Johnson, P. B.; Christy, R. W. Optical constants of the noble metals. *Phys. Rev. B* **1972**, *6*, 4370−4379.
(44) Li, C.; Luo, H.; Hou, L.; Wang, Q.; Liu, K.; Gan, X.; Zhao, J.; Xiao, F. Giant photoluminescence enhancement of monolayer WSe_2 using a plasmonic nanocavity with on-demand resonance. *Nano Lett.* **2024**, *24*, 5879−5885.
(45) Ciraci, C.; Rose, A.; Argyropoulos, C.; Smith, D. R. Numerical studies of the modification of photodynamic processes by film-coupled plasmonic nanoparticles. *J. Opt. Soc. Am. B* **2014**, *31*, 2601−2607.
(46) Zhang, R.; Koutsos, V.; Cheung, R. Elastic properties of suspended multilayer WSe_2. *Appl. Phys. Lett.* **2016**, *108*, No. 042104.

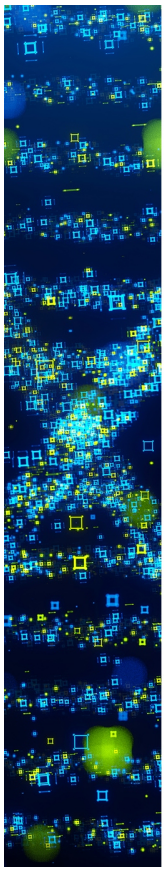

https://doi.org/10.1021/acsnano.5c21481
ACS Nano 2026, 20, 6279−6286